Variable temperature probing of minority carrier transport and optical properties in *p*-Ga_2O_3

Sushrut Modak [a)], Leonid Chernyak [a,g)], Alfons Schulte [a)], Corinne Sartel [b)], Vincent Sallet [b)], Yves Dumont [b)], Ekaterine Chikoidze [b)], Xinyi Xia [c)], Fan Ren [c)], Stephen J. Pearton [d)], Arie Ruzin [e)], Denis M. Zhigunov [f)], Sergey S. Kosolobov [f)], Vladimir P. Drachev [f)]

[a] *Department of Physics, University of Central Florida, Orlando, FL 32816, USA*

[b] *Groupe d'Etude de la Matière Condensée, Université Paris-Saclay, Université de Versailles Saint Quentin en Yvelines – CNRS, 45 Av. des Etats-Unis, 78035 Versailles Cedex, France*

[c] *Department of Chemical Engineering, University of Florida, Gainesville, FL 32611, USA*

[d] *Material Science and Engineering, University of Florida, Gainesville, FL 32611, USA*

[e] *School of Electrical Engineering, Tel Aviv University, Tel Aviv 69978, Israel*

[f] *Skolkovo Inst Sci & Technol, Ctr Eng. Physics, Nobel St, Bldg 1, Moscow 121205, Russia*

Electron Beam-Induced Current in the temperature range from 304 K to 404 K was employed to measure the minority carrier diffusion length in Metal-Organic Chemical Vapor Deposition-grown p-Ga_2O_3 thin films with two different concentrations of majority carriers. The diffusion length of electrons exhibited a decrease with increasing temperature. Additionally, the cathodoluminescence emission spectrum identified optical signatures of the acceptor levels associated with V_{Ga}^{-} -V_O^{++} complex. The activation energies for diffusion length decrease and quenching of cathodoluminescence emission with increasing temperature were ascribed to the thermal de-trapping of electrons from V_{Ga}^{-} -V_O^{++} defect complexes.

[g)] email: chernyak@physics.ucf.edu

β-Ga_2O_3 is an emerging fourth-generation power electronics platform with a wide-bandgap of ~ 4.8 eV and a high breakdown field (8 x 10^6 Vcm^{-1}) [1-6]. It is becoming increasingly attractive due to its applications in high-power electronics, true solar-blind UV detection, and optoelectronic devices [2, 3, 7-10]. Undoped β-Ga_2O_3 tends to be n-type due to unintentional donor impurities such as Si. Intentionally n-type β-Ga_2O_3 can be obtained by adding controlled amounts of impurities such as Si, Sn, and Ge, which is well documented [3, 5]. Carrier transport characterization revealed impurity bands and the hopping mechanism of electrical transport in such doped films [11-14]. Low-temperature electron mobilities up to 796 cm^2/Vs [13] have been reported. The incorporation of doped layers in devices such as Schottky diodes, field-effect transistors (FETs), including metal-oxide FETs (MOSFETs) and their ability to withstand high energy particle radiation have been explored [15-24]. Replicating these results to achieve p-type conductivity in β-Ga_2O_3 has proven very difficult due to factors such as doping asymmetry, high compensation of acceptors, the high ionization energy of acceptor levels, and hole-trapping at O(I) and O(II) sites [25-30]. Despite these difficulties, native p-type conductivity was demonstrated at high temperatures in undoped β-Ga_2O_3 [31, 32]. It was observed that native p-type conductivity is achievable by creating a significant number of native acceptors (V_{Ga}) and suppressing the compensation due to native donors (V_O). The thermodynamic balance required to weaken the self-compensation in undoped β-Ga_2O_3 was achieved by adjusting the growth temperatures and oxygen partial pressures during the deposition of Ga_2O_3 on sapphire substrates by Metal-Organic Chemical Vapor Deposition (MOCVD) [32, 33].

P-type β-Ga_2O_3 is a relatively recent discovery and an uncharted territory in terms of minority carrier transport and luminescence characterization as well as their temperature dependences. Knowledge of minority carrier (electrons) transport properties in p-type β-Ga_2O_3 is

essential for achieving bipolar technology on the gallium oxide platform. In this report, the diffusion length of minority carriers (electrons), cathodoluminescence, and their temperature dependence are studied in p-type β-Ga_2O_3 with two different majority carrier (holes) concentrations.

Undoped β-Ga_2O_3 samples, analyzed in this study, were grown in an RF-heated horizontal MOCVD reactor with separate inlets to avoid premature reactions in the manifold between oxygen and organometallics precursors. Trimethylgallium (TMGa) and 5.5 N pure oxygen were used as gallium and oxygen sources, respectively. Argon was used as the carrier gas (cf. ref. [32]). The β-Ga_2O_3 layer was grown on a c-oriented sapphire substrate using Ga/O ratio and growth temperature as 1.4×10^{-4} and 775 °C, respectively. Two different total reactor pressures of 30 and 38 Torr and variable growth rates (gallium and oxygen precursor fluxes) were used to create two different native defect (V_{Ga} and V_O) concentrations in the Ga_2O_3 films, leading to the different values of p-type conductivity. The difference between the total reactor pressure for the deposition of the two samples is due to a change in the oxygen partial pressure. The concentration of native defects responsible for p-type conductivity is sensitive to the oxygen partial pressure. The epitaxial layer thickness was ~ 450 nm. X-ray diffraction scans revealed highly textured films of gallium oxide in the β-Ga_2O_3 phase with monoclinic space group (*C2/m*) symmetry. Further in the text, the sample grown under 30 Torr total reactor pressure will be labeled as A and grown under 38 Torr as B.

A detailed study of the electrical transport properties for the above-referenced highly resistive (close to stochiometric) Ga_2O_3 samples has been performed. Ohmic contacts were prepared with silver paint at the four corners of the sample. Hall Effect measurements were conducted in a Van der Pauw configuration in the 500-850 K temperature range for magnetic fields

perpendicular to the film plane varying from -1.6 to 1.6 T, using a high impedance high-temperature custom-designed measurement set-up. Resistivities at highest measured T = 850 K were found to be ρ (A) = 1.2 x 10^3 Ohm·cm and ρ (B) = 1.3 x 10^4 Ohm·cm. Hall Effect measurements demonstrated (cf. [31, 32]) the positive sign for majority carriers in both samples, thus confirming the p-type conductivity. The free hole concentrations and mobilities at 850 K were estimated as follows: p = 5.6 x 10^{14} cm^{-3}; μ = 8.0 $cm^2V^{-1}s^{-1}$ for the sample A and p = 2.7 x 10^{13} cm^{-3} and μ = 16 $cm^2V^{-1}s^{-1}$ for the sample B. Temperature-dependent measurements were possible to perform only down to 520 K (p = 2.0 x 10^{10} cm^{-3}) for A and only to 620 K for B sample (p = 7.1 x 10^{10} cm^{-3}), due to the samples high resistivity. The difference in hole concentrations is due to the difference in growth conditions (total reactor pressure and the ratio of gallium-oxygen precursor fluxes) resulting in the variation of electrical compensation degree $K = N_A/N_D$, *i.e.*, the ratio of native acceptor to native donor concentrations. Ni/Au (20 nm/ 80 nm) asymmetrical pseudo-Schottky contacts were created on the film with lithography/liftoff techniques for further analysis.

Electron Beam-Induced Current (EBIC) and Cathodoluminescence (CL) measurements were performed *in-situ* in a Phillips XL-30 Scanning Electron Microscope (SEM) to characterize the diffusion length (L) of minority carriers (electrons) and luminescence behavior of the samples, respectively. The measurements were carried out in the 304-404 K temperature range using a Gatan MonoCL2 temperature-controlled stage integrated into the SEM. For both EBIC and CL measurements, the electron beam energy was kept at 10 keV. The EBIC line scans were obtained in a planar configuration (Fig. 1). The EBIC signal was amplified with a Stanford Research Systems SR 570 low-noise current amplifier and digitized with a Keithley DMM 2000 controlled by a PC using homemade software. CL measurements were carried out using a Gatan MonoCL2

attachment to the SEM. Spectra were recorded with a Hamamatsu photomultiplier tube sensitive in 150-850 nm range and a single grating monochromator (blazed at 1200 lines/mm).

EBIC line-scans were used to extract diffusion length, L, from the following equation [34, 35]:

$$C(x) = C_0 x^{\alpha} \exp\left(-\frac{x}{L}\right). \quad (1)$$

Here, C(x) is the EBIC signal at distance x from the Schottky junction, C_0 is a scaling constant, x is the distance of the electron beam from the Schottky barrier, α is the linearization parameter, related to surface recombination velocity. The coefficient α was set at -0.5, corresponding to the low influence of surface recombination. Since the carrier concentration is low in both samples, the Schottky barrier depletion width is significantly larger than L and, therefore, the approach outlined in ref. [36] was used. Figs. 2a and 2b show the raw EBIC signals and a fit with $x^{\alpha}\exp(-x/L)$ used in extracting L for the samples A and B, respectively. The temperature dependence of L for samples A and B is shown in Fig. 3. L decreased with increasing temperature, with values for the samples A and B at 304 K of 1040 nm and 8506 nm, respectively. At 404 K, L reduced to 640 nm and 6193 nm, respectively. Relatively large values of L are partially due to the shallow majority carrier concentration. Within the current temperature range of measurements, the origin of L decrease is likely due to phonon scattering [37]. Reported values of L for minority carrier (holes) in n-type β-Ga_2O_3 are within 50 nm – 600 nm [20, 21, 38-41], lower than those of electrons measured in this work for minority carrier electrons. A likely reason could be the large effective mass for holes (18-25 m_0) [42]. It is worth noting that a similar dependence of L on temperature was found for n-type β-Ga_2O_3, but it is attributed to scattering on ionized impurities due to heavy Si doping [41]. The activation energy for the temperature dependence of L is given by [43, 44]

$$L(T) = L_0 \exp\left(\frac{\Delta E_{L,T}}{2kT}\right). \quad (2)$$

Here, L_0 is a scaling constant, $\Delta E_{L,T}$ is the thermal activation energy, k is the Boltzmann constant, and T is the temperature. The activation energy pertaining to the reduction of L with temperature is 67 meV and 113 meV for samples A and B, respectively. A detailed discussion regarding the origin of $\Delta E_{L,T}$ is given later in the text.

Raw CL spectra and their Gaussian decompositions at 304 K are presented in Figs. 4a and 4b for samples A and B, respectively. The CL spectra exhibit four characteristic luminescence bands: ultraviolet (UVL' and UVL) at 375 nm and 415nm; blue (BL) at 450 nm; and green (GL) at 520 nm. The UVL' and UVL bands are commonly ascribed to recombination of self-trapped excitons, considering the absence of near band edge emission and their lack in β-Ga_2O_3 for sub-bandgap excitation [26, 27, 29, 45-48]. The self-localization of excitons occurs at O(I) and O(II) site, corresponding to UVL' and UVL bands, respectively [47, 49]. Although, as has been shown from Electron Paramagnetic Resonance (EPR) measurements [50] and confirmed by several independent EBIC studies on n-type β-Ga_2O_3 [20-23, 39, 51, 52], the self-localization of holes is unstable above 110 K, the optical signature of the self-trapped excitons persists in CL and photoluminescence (PL) measurements. Note that the relative contribution of UVL' and UVL bands in both A and B samples are much lower than in n-type β-Ga_2O_3, found in earlier reports [26, 47, 49, 53-58]. The BL band arises from donor-acceptor pair recombination involving a V_O donor and V_{Ga} or a (V_O, V_{Ga}) complex as an acceptor. GL has several different origins, mentioned in the literature, and was observed with an array of various dopants such as Mg [59], Si [54], and Er [60]. In undoped β-Ga_2O_3, grown by floating zone technique, Villora *et al*. [61] ascribed GL to self-trapped excitons as it existed only for PL excitation energies below the bandgap. Moreover, this band was also observed in β-Ga_2O_3 nanoflakes, structurally consisting of a crystalline core and

amorphous shell [62, 63]. In a recent study on β-Ga_2O_3 films on a c-plane sapphire substrate with (201) orientation, deposited with magnetron sputtering [64], the intensities of BL and GL were modulated by changing oxygen flow rate, and the origin of the GL was attributed to the presence of isolated V_{Ga}. Furthermore, the presence of isolated V_O did not independently play a role in enhancing BL, and the origin of BL was assigned to a defect complex involving V_O and V_{Ga}. Given the abundance of isolated V_{Ga} acceptors and (V_O, V_{Ga}) complexes in both samples, a relatively large contribution of both BL and GL to the CL emission spectrum is observed in this work. Binet and Gourier [53] and Onuma *et al.* [49] independently found a correlation between conductivity and concentration of the V_O donors in n-type β-Ga_2O_3. In this case, since V_O compensates the acceptors, and due to the high ionization energy of acceptors, p-type β-Ga_2O_3 has relatively high resistivity below 450 K [31, 32]. The presence of a rather large number of V_{Ga} acceptors and (V_O, V_{Ga}) acceptor complexes, promoting p-type conductivity, was confirmed from the CL emission spectrum.

The temperature dependence of the CL signal follows the form [53]

$$I(T) = I_0/(1 + e^{\Delta E_{CL}/kT}). \quad (3)$$

Here, I(T) is the integrated CL intensity, I_0 is a constant, and ΔE_{CL} is the process activation energy. Fig. 5 shows the Arrhenius plot of $\ln(I_0/I(T) - 1)$. The process activation energy ΔE_{CL}, obtained from a linear fit of the temperature dependence depicted in Fig. 5, was 88 meV and 101 meV for samples A and B, respectively. The total CL intensity is used in Fig. 5 because the relative contributions of the individual luminescence bands remained approximately constant in the temperature range of the measurements. The activation energies $\Delta E_{L,T}$ and ΔE_{CL} for sample A (67 meV and 88 meV, respectively) and sample B (113 meV and 101 meV, respectively) are comparable and can be attributed to a common origin.

Temperature-dependent resistivity measurements between 300 K to 850 K in our earlier study [32] on deep V_{Ga} acceptor defects in similar Ga_2O_3 samples showed two activation energies due to temperature-activated processes. In the high temperature region (T > 400 K), the acceptors are ionized with an activation energy of 0.56 eV. But for temperatures between 300 K and 400 K, a shallower V_{Ga}^{-} -V_O^{++} acceptor complex is present. The concentration of this complex strongly increases in off stochiometric samples (after oxygen post-annealing) detectable by Hall Effect. The electrical activation energy has been determined as 0.17 eV (170 meV), and these complexes are responsible for forming an impurity band and hopping conductivity below 400 K [32]. It is suggested in the present study that the non-equilibrium electrons in as-grown (close to stoichiometry) Ga_2O_3 thin films, generated during the excitation with an electron beam, are captured by V_{Ga}^{-} -V_O^{++} acceptor defect complexes. The thermal emission of these captured electrons is represented by activation energies extracted from EBIC and CL experiments. In other words, V_{Ga}^{-} -V_O^{++} acceptor complexes are detectable by electron beam excitation even in close to stochiometric samples when electrical measurements are insensitive, probably due to their insufficient concentration. Moreover, based on the discussion given above, the nature of the native defects probed with EBIC and CL in both samples is alike. The difference in the activation energies is primarily due to the difference in their concentration, which is governed by the oxygen partial pressure during the growth process. The process of non-equilibrium electron de-trapping in this work has an analogy with Mg-doped p-GaN, where the release of a non-equilibrium electron from deep acceptor levels is seen in the thermal activation of L [65].

In summary, EBIC and CL techniques were employed to understand the temperature dependence of the diffusion length of minority carriers and CL emission in p-type β-Ga_2O_3 with two different hole concentrations. Optical signatures of native acceptor defects (isolated V_{Ga} and

V_{Ga}^{-} -V_O^{2+} complex) were identified in the CL spectrum. Additionally, the activation energies for change of L with temperature ($\Delta E_{L,\,T}$) and thermal quenching of CL intensity (ΔE_{CL}) were experimentally obtained as 67 meV and 88 meV for sample A and 113 meV and 101 meV for sample B, respectively, within the temperature range of 304 K to 404 K. Comparable values of $\Delta E_{L,T}$ and ΔE_{CL} indicate a common origin for both processes, which is attributed to the thermal de-trapping of electrons from V_{Ga}^{-} -V_O^{++} acceptor level. The current development in the characterization of p-type β-Ga_2O_3 could serve a pivotal role in realizing bipolar gallium oxide devices.

Acknowledgments

The research at UCF was supported in part by NSF (ECCS1802208 and ECCS2127916). Research at UCF and Tel Aviv University was supported partially by the US-Israel BSF (award # 2018010) and NATO (award # G5748). The work at UF was performed as part of the Interaction of Ionizing Radiation with Matter University Research Alliance (IIRM-URA), sponsored by the Department of the Defense, Defense Threat Reduction Agency under award HDTRA1-20-2-0002, monitored by Jacob Calkins and by NSF DMR 1856662 (J.H. Edgar). The present work is a part of the "GALLIA" International Research Project, CNRS, France.

Data Availability

The data that support the findings of this study are available from the corresponding author upon reasonable request.

References

1. S.I. Stepanov, V. I. Nikolaev, V. E. Bougrov, and A. E. Romanov, Rev. Adv. Mater. Sci. **44**, 63 (2016).
2. M. Kim, J.-H. Seo, U. Singisetti, and Z. Ma, J. Mater. Chem. C **5**, 8338 (2017).
3. S.J. Pearton, J. Yang, P.H. Cary, F. Ren, J. Kim, M.J. Tadjer, and M.A. Mastro, Appl. Phys. Rev. **5**, 011301 (2018).
4. *Progress in semiconductor β-Ga2O3*, in *Ultra-Wide Bandgap Semiconductor Materials*, M. Liao, B. Shen, and Z. Wang, Editors, Elsevier, 263-345 (2019).
5. M.J. Tadjer, J.L. Lyons, N. Nepal, J.A. Freitas, A.D. Koehler, and G.M. Foster, ECS J. Solid State Sci. Technol. **8**, Q3187 (2019).
6. J. Zhang, J. Shi, D.-C. Qi, L. Chen, and K.H.L. Zhang, APL Mater. **8**, 020906 (2020).
7. J.Y. Tsao, S. Chowdhury, M.A. Hollis, D. Jena, N.M. Johnson, K.A. Jones, R.J. Kaplar, S. Rajan, C.G. Van de Walle, E. Bellotti, C.L. Chua, R. Collazo, M.E. Coltrin, J.A. Cooper, K.R. Evans, S. Graham, T.A. Grotjohn, E.R. Heller, M. Higashiwaki, M.S. Islam, P.W. Juodawlkis, M.A. Khan, A.D. Koehler, J.H. Leach, U.K. Mishra, R.J. Nemanich, R.C.N. Pilawa-Podgurski, J.B. Shealy, Z. Sitar, M.J. Tadjer, A.F. Witulski, M. Wraback, and J.A. Simmons, Adv. Electron. Mater. **4**, 1600501 (2018).
8. H. von Wenckstern, Adv. Electron. Mater. **3**, 1600350 (2017).
9. M. Higashiwaki, K. Sasaki, H. Murakami, Y. Kumagai, A. Koukitu, A. Kuramata, T. Masui, and S. Yamakoshi, Semicond. Sci. Technol. **31**, 034001 (2016).
10. K. Akito, K. Kimiyoshi, W. Shinya, Y. Yu, M. Takekazu, and Y. Shigenobu, Jpn. J. Appl. Phys. **55**, (2016).
11. H.J. Von Bardeleben and J.L. Cantin, J. Appl. Phys. **128**, (2020).
12. E.B. Yakimov, A.Y. Polyakov, N.B. Smirnov, I.V. Shchemerov, P.S. Vergeles, E.E. Yakimov, A.V. Chernykh, M. Xian, F. Ren, and S.J. Pearton, J. Phys. D **53**, 495108 (2020).

13. A.K. Rajapitamahuni, L.R. Thoutam, P. Ranga, S. Krishnamoorthy, and B. Jalan, Appl. Phys. Lett. **118**, (2021).
14. Z. Kabilova, C. Kurdak, and R.L. Peterson, Semicond. Sci. Technol. **34**, 03lt02 (2019).
15. A.J. Green, K.D. Chabak, E.R. Heller, R.C. Fitch, M. Baldini, A. Fiedler, K. Irmscher, G. Wagner, Z. Galazka, S.E. Tetlak, A. Crespo, K. Leedy, and G.H. Jessen, IEEE Electr. Device L. **37**, 902 (2016).
16. M.H. Wong, K. Sasaki, A. Kuramata, S. Yamakoshi, and M. Higashiwaki, IEEE Electr. Device L. **37**, 212 (2016).
17. H. Masataka, K. Akito, M. Hisashi, and K. Yoshinao, J. Phys. D **50**, 333002 (2017).
18. G. Yang, S. Jang, F. Ren, S.J. Pearton, and J. Kim, ACS Appl. Mater. Interfaces **9**, 40471 (2017).
19. K. Konishi, K. Goto, H. Murakami, Y. Kumagai, A. Kuramata, S. Yamakoshi, and M. Higashiwaki, Appl. Phys. Lett. **110**, 103506 (2017).
20. S. Modak, L. Chernyak, S. Khodorov, I. Lubomirsky, J. Yang, F. Ren, and S.J. Pearton, ECS J. Solid State Sci. Technol. **8**, Q3050 (2019).
21. S. Modak, J. Lee, L. Chernyak, J. Yang, F. Ren, S.J. Pearton, S. Khodorov, and I. Lubomirsky, AIP Adv. **9**, 015127 (2019).
22. S. Modak, L. Chernyak, S. Khodorov, I. Lubomirsky, A. Ruzin, M. Xian, F. Ren, and S.J. Pearton, ECS J. Solid State Sci. Technol. **9**, 045018 (2020).
23. S. Modak, L. Chernyak, A. Schulte, M. Xian, F. Ren, S.J. Pearton, I. Lubomirsky, A. Ruzin, S.S. Kosolobov, and V.P. Drachev, Appl. Phys. Lett. **118**, 202105 (2021).
24. S. Modak, L. Chernyak, A. Schulte, M. Xian, F. Ren, S.J. Pearton, A. Ruzin, S.S. Kosolobov, and V.P. Drachev, AIP Adv. **11**, 125014 (2021).
25. Y. Yan and S.H. Wei, Physica Status Solidi B-Basic Solid State Physics **245**, (2008).
26. H. Gao, S. Muralidharan, N. Pronin, M.R. Karim, S.M. White, T. Asel, G. Foster, S. Krishnamoorthy, S. Rajan, L.R. Cao, M. Higashiwaki, H. von Wenckstern, M. Grundmann, H. Zhao, D.C. Look, and L.J. Brillson, Appl. Phys. Lett. **112**, 242102 (2018).

27. S. Marcinkevičius and J.S. Speck, Appl. Phys. Lett. **116**, 132101 (2020).
28. M.D. McCluskey, J. Appl. Phys. **127**, (2020).
29. Y.K. Frodason, K.M. Johansen, L. Vines, and J.B. Varley, J. Appl. Phys. **127**, 075701 (2020).
30. T.D. Gustafson, J. Jesenovec, C.A. Lenyk, N.C. Giles, J.S. McCloy, M.D. McCluskey, and L.E. Halliburton, J. Appl. Phys. **129**, 155701 (2021).
31. E. Chikoidze, A. Fellous, A. Perez-Tomas, G. Sauthier, T. Tchelidze, C. Ton-That, T.T. Huynh, M. Phillips, S. Russell, M. Jennings, B. Berini, F. Jomard, and Y. Dumont, Mater. Today Phys. **3**, 118 (2017).
32. E. Chikoidze, C. Sartel, H. Mohamed, I. Madaci, T. Tchelidze, M. Modreanu, P. Vales-Castro, C. Rubio, C. Arnold, V. Sallet, Y. Dumont, and A. Perez-Tomas, J. Mater. Chem. C **7**, 10231 (2019).
33. X. Wang, T. Liu, Y. Lu, Q. Li, R. Guo, X. Jiao, and X. Xu, J. Phys. Chem. Solids **132**, (2019).
34. C.A. Dimitriadis, J. Phys. D **14**, 2269 (1981).
35. L. Chernyak, A. Osinsky, H. Temkin, J.W. Yang, Q. Chen, and M. Asif Khan, Appl. Phys. Lett. **69**, 2531 (1996).
36. V.K.S. Ong, O. Kurniawan, G. Moldovan, and C.J. Humphreys, J. Appl. Phys. **100**, 114501 (2006).
37. N. Ma, N. Tanen, A. Verma, Z. Guo, T. Luo, H. Xing, and D. Jena, Appl. Phys. Lett. **109**, 212101 (2016).
38. A.Y. Polyakov, I.-H. Lee, N.B. Smirnov, E.B. Yakimov, I.V. Shchemerov, A.V. Chernykh, A.I. Kochkova, A.A. Vasilev, F. Ren, P.H. Carey, and S.J. Pearton, Appl. Phys. Lett. **115**, 032101 (2019).
39. A.Y. Polyakov, N.B. Smirnov, I.V. Shchemerov, E.B. Yakimov, S.J. Pearton, C. Fares, J. Yang, F. Ren, J. Kim, P.B. Lagov, V.S. Stolbunov, and A. Kochkova, Appl. Phys. Lett. **113**, 092102 (2018).

40. E.B. Yakimov, A.Y. Polyakov, N.B. Smirnov, I.V. Shchemerov, J. Yang, F. Ren, G. Yang, J. Kim, and S.J. Pearton, J. Appl. Phys. **123**, 185704 (2018).
41. J. Lee, E. Flitsiyan, L. Chernyak, J. Yang, F. Ren, S.J. Pearton, B. Meyler, and Y.J. Salzman, Appl. Phys. Lett. **112**, 082104 (2018).
42. M.M.R. Adnan, D. Verma, Z. Xia, N.K. Kalarickal, S. Rajan, and R.C. Myers, Phys. Rev. Appl. **16**, (2021).
43. O. Lopatiuk-Tirpak, L. Chernyak, F.X. Xiu, J.L. Liu, S. Jang, F. Ren, S.J. Pearton, K. Gartsman, Y. Feldman, A. Osinsky, and P. Chow, J. Appl. Phys. **100**, 086101 (2006).
44. M. Eckstein and H.U. Habermeier, J. Phys. IV **01**, C6-23 (1991).
45. S. Yamaoka and M. Nakayama, Phys. Status Solidi C **13**, 93 (2016).
46. P. Deák, Q. Duy Ho, F. Seemann, B. Aradi, M. Lorke, and T. Frauenheim, Phys. Rev. B **95**, 075208 (2017).
47. Q.D. Ho, T. Frauenheim, and P. Deák, Phys. Rev. B **97**, 115163 (2018).
48. J. Lapp, D. Thapa, J. Huso, A. Canul, M. McCluskey, and L. Bergman. Bull. Am. Phys. Soc. (2020).
49. T. Onuma, S. Fujioka, T. Yamaguchi, M. Higashiwaki, K. Sasaki, T. Masui, and T. Honda, Appl. Phys. Lett. **103**, 041910 (2013).
50. B.E. Kananen, N.C. Giles, L.E. Halliburton, G.K. Foundos, K.B. Chang, and K.T. Stevens, J. Appl. Phys. **122**, 215703 (2017).
51. A.Y. Polyakov, I.-H. Lee, N.B. Smirnov, A.V. Govorkov, E.A. Kozhukhova, N.G. Kolin, A.V. Korulin, V.M. Boiko, and S.J. Pearton, J. Appl. Phys. **109**, 123703 (2011).
52. E.B. Yakimov, A.Y. Polyakov, I.V. Shchemerov, N.B. Smirnov, A.A. Vasilev, P.S. Vergeles, E.E. Yakimov, A.V. Chernykh, F. Ren, and S.J. Pearton, Appl. Phys. Lett. **118**, (2021).
53. L. Binet and D. Gourier, J. Phys. Chem. Solid **59**, 1241 (1998).
54. K. Shimamura, E.G. Víllora, T. Ujiie, and K. Aoki, Appl. Phys. Lett. **92**, 201914 (2008).
55. S. Yamaoka, Y. Furukawa, and M. Nakayama, Phys. Rev. B **95**, 094304 (2017).

56. T.T. Huynh, L.L.C. Lem, A. Kuramata, M.R. Phillips, and C. Ton-That, Phys. Rev. Mater. **2**, 105203 (2018).

57. T. Onuma, Y. Nakata, K. Sasaki, T. Masui, T. Yamaguchi, T. Honda, A. Kuramata, S. Yamakoshi, and M. Higashiwaki, J. Appl. Phys. **124**, 075103 (2018).

58. Y. Wang, P.T. Dickens, J.B. Varley, X. Ni, E. Lotubai, S. Sprawls, F. Liu, V. Lordi, S. Krishnamoorthy, S. Blair, K.G. Lynn, M. Scarpulla, and B. Sensale-Rodriguez, Sci. Rep. **8**, 18075 (2018).

59. V. Vasyltsiv, A. Luchechko, L. Kostyk, and B. Pavlyk. 2019 XIth International Scientific and Practical Conference on Electronics and Information Technologies (ELIT). (2019).

60. E. Nogales, J.A. García, B. Méndez, J. Piqueras, K. Lorenz, and E. Alves, J. Phys. D **41**, 065406 (2008).

61. E.G. Víllora, M. Yamaga, T. Inoue, S. Yabasi, Y. Masui, T. Sugawara, and T. Fukuda, Jpn. J. Appl. Phys. **41**, L622 (2002).

62. X.T. Zhou, F. Heigl, J.Y.P. Ko, M.W. Murphy, J.G. Zhou, T. Regier, R.I.R. Blyth, and T.K. Sham, Phys. Rev. B **75**, (2007).

63. G. Pozina, M. Forsberg, M.A. Kaliteevski, and C. Hemmingsson, Sci Rep **7**, (2017).

64. Y. Nie, S. Jiao, S. Li, H. Lu, S. Liu, S. Yang, D. Wang, S. Gao, J. Wang, and Y. Li, J. Alloys Compd, 163431 (2021).

65. L. Chernyak, A. Osinsky, V. Fuflyigin, and E.F. Schubert, Appl. Phys. Lett. **77**, 875 (2000).

Figure Captions

Figure 1: A schematic diagram of the sample structure and experimental set-up.

Figure 2: An example of the acquired EBIC line-scan from sample A **(a)** and sample B **(b)** at 304 K along with $exp(-x/L)/x^{0.5}$ fit for extraction of the diffusion length.

Figure 3: Temperature dependence of the diffusion length for the samples A and B. **Inset:** Arrhenius plot with a linear fit for extraction of the activation energy $\Delta E_{L,T}$.

Figure 4: Normalized CL spectrum for sample A **(a)** and sample B **(b)** and their Gaussian decomposition into four bands- UVL', UVL BL, and GL.

Figure 5: Arrhenius plot of $\ln(I_0/I(T) - 1)$ vs. $1/(kT)$ from Eqn. (1), where I is the integrated CL emission intensity, with the fit, used in the extraction of activation energy (ΔE_{CL}) for the thermal quenching process.

337 **Figure 1**

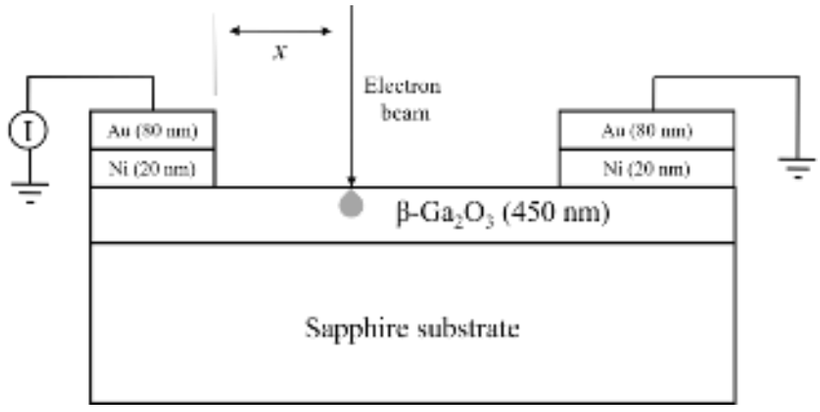

338

339

340 **Figure 2**

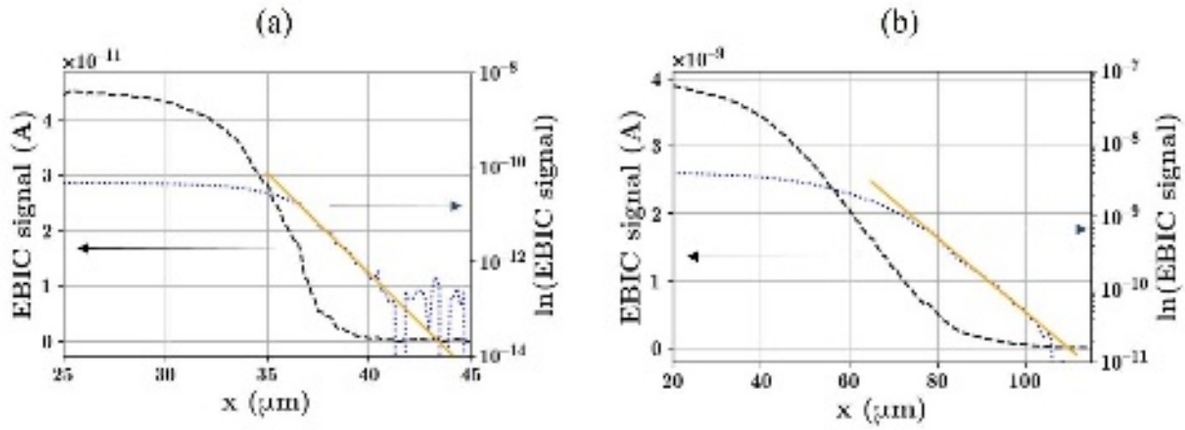

341

342

343 **Figure 3**

344

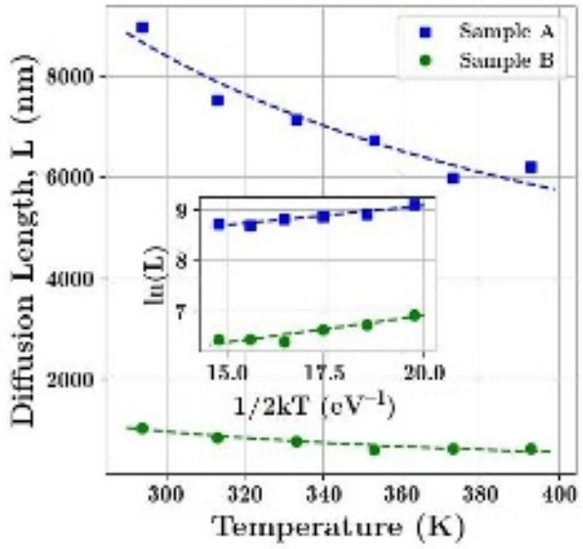

345

346 **Figure 4**

347

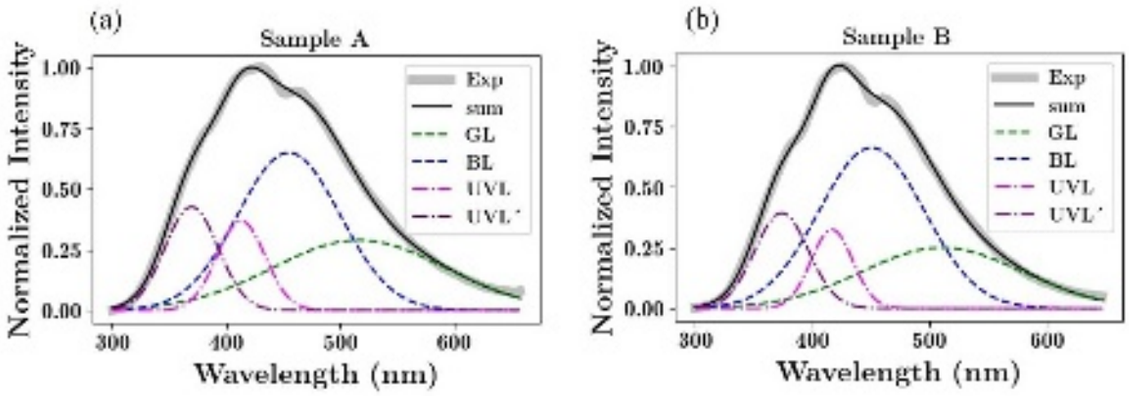

348

349 **Figure 5**

350

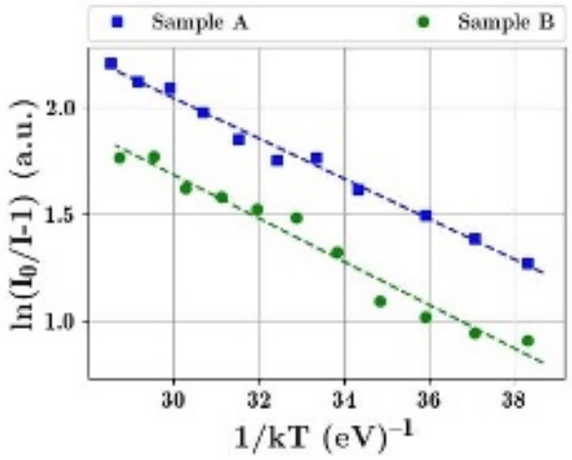

351

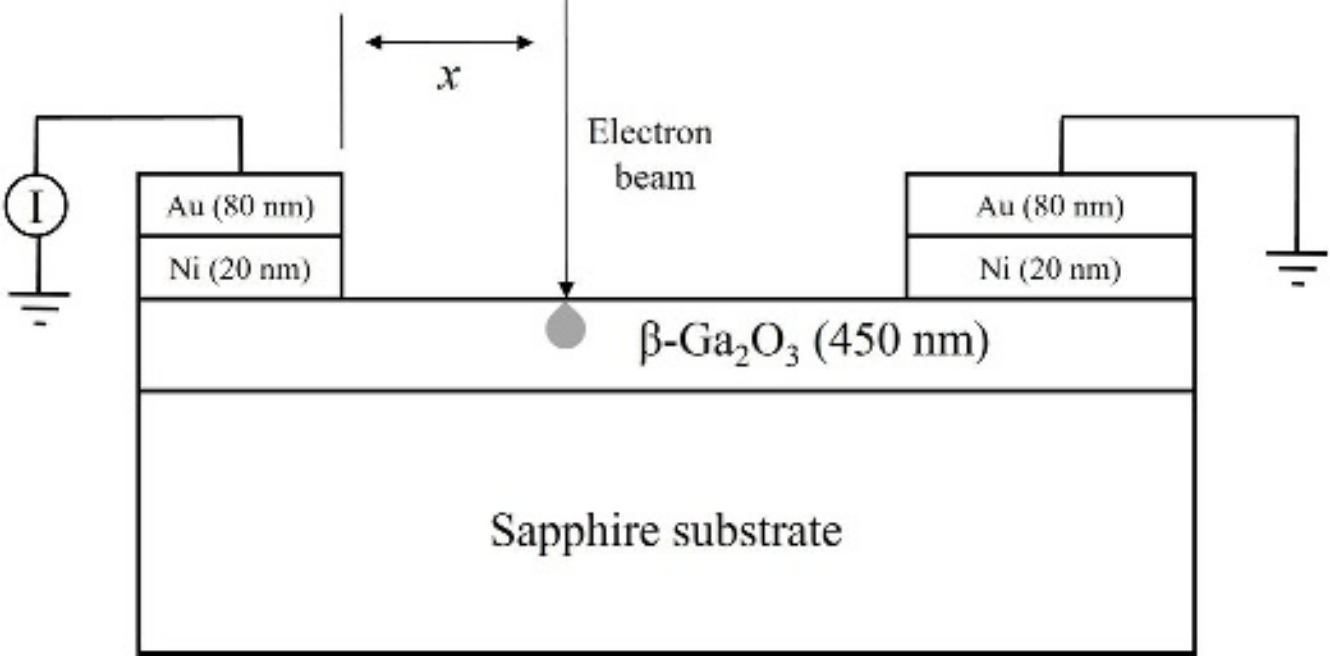
x
Electron beam
I
Au (80 nm)
Ni (20 nm)
Au (80 nm)
Ni (20 nm)
β-Ga2O3 (450 nm)
Sapphire substrate

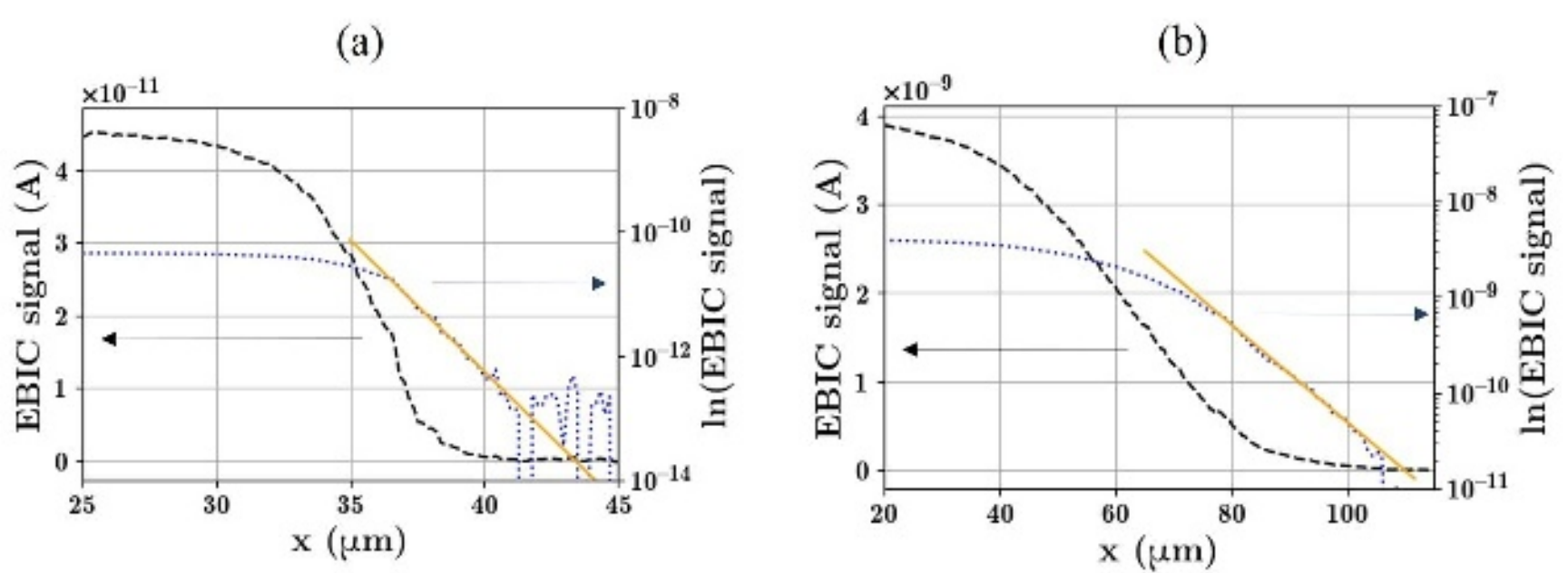
(a)
×10⁻¹¹
EBIC signal (A)
ln(EBIC signal)
x (μm)
(b)
×10⁻⁹
EBIC signal (A)
ln(EBIC signal)
x (μm)

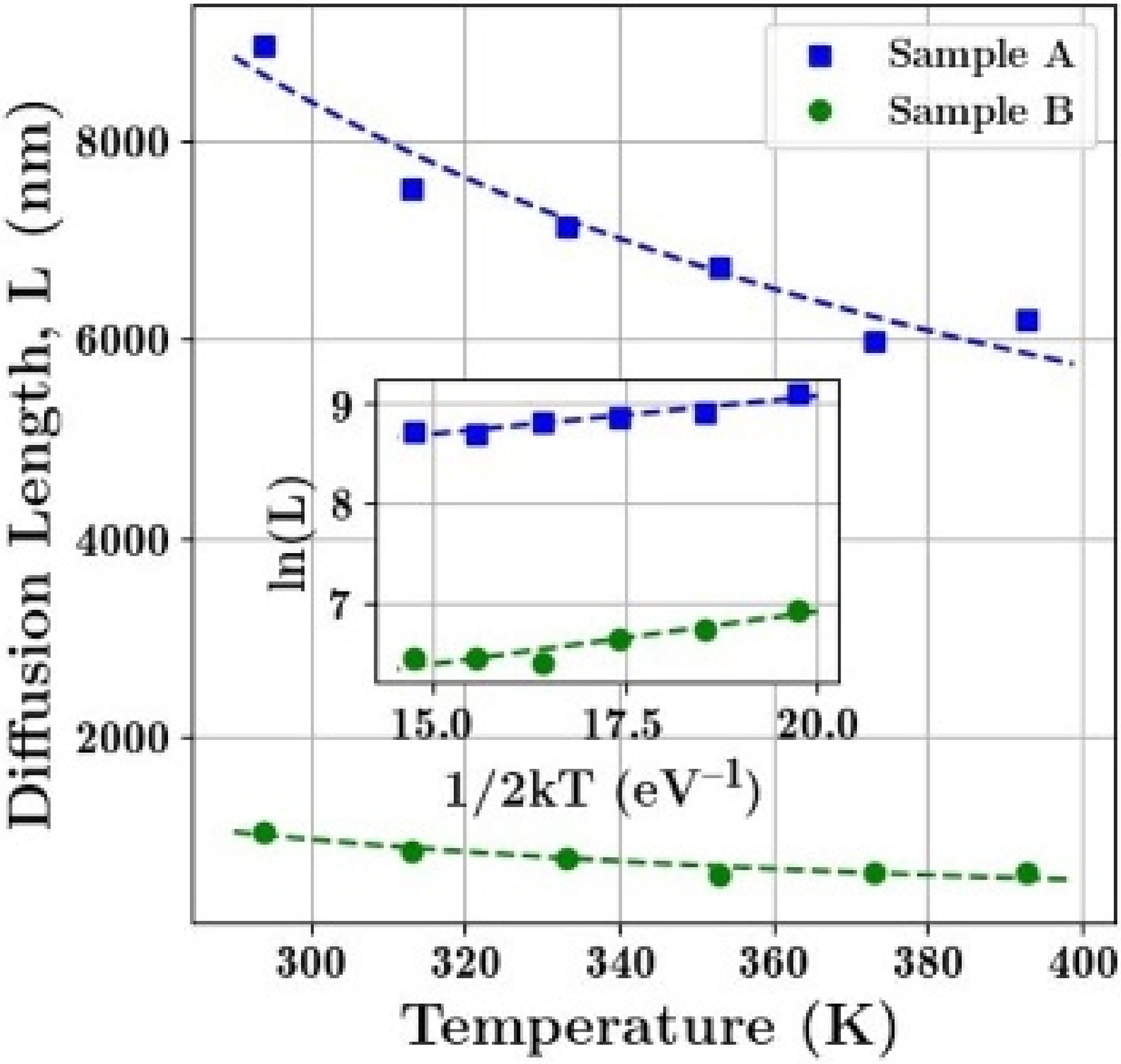
Sample A
Sample B
Diffusion Length, L (nm)
8000
6000
4000
2000
300
320
340
360
380
400
Temperature (K)
ln(L)
9
8
7
15.0
17.5
20.0
1/2kT (eV^{-1})

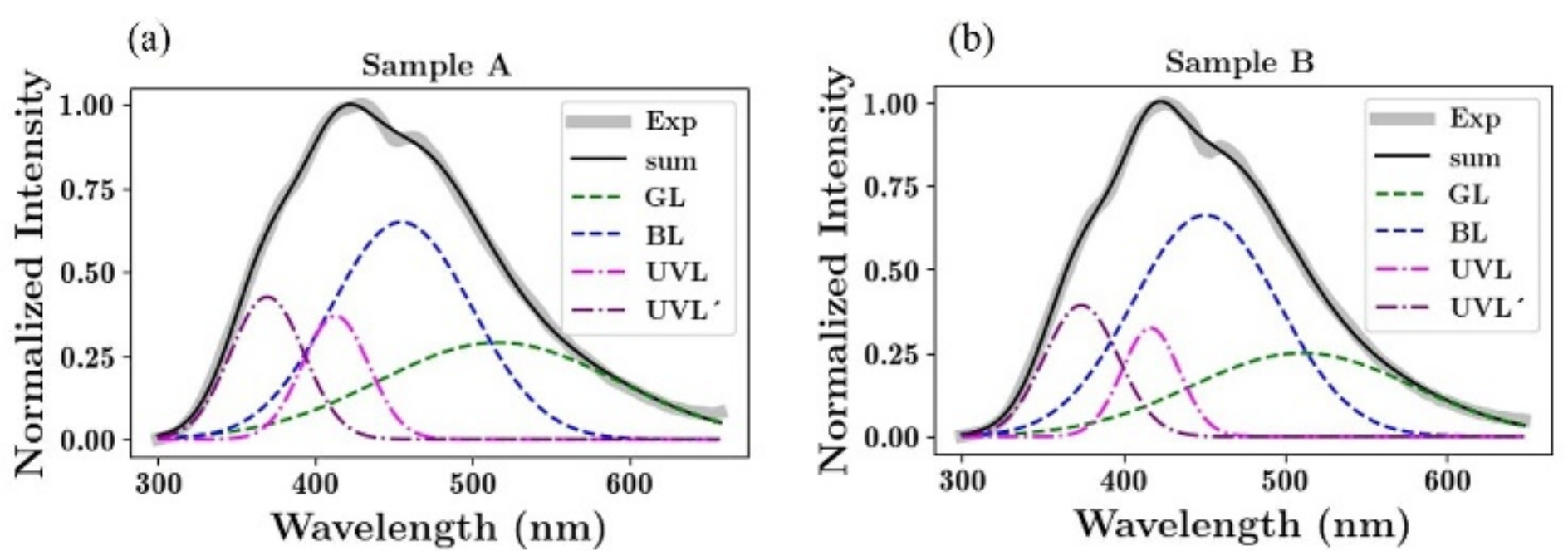
(a)
Sample A
Normalized Intensity
1.00
0.75
0.50
0.25
0.00
300
400
500
600
Wavelength (nm)
Exp
sum
GL
BL
UVL
UVL´
(b)
Sample B
Normalized Intensity
1.00
0.75
0.50
0.25
0.00
300
400
500
600
Wavelength (nm)
Exp
sum
GL
BL
UVL
UVL´

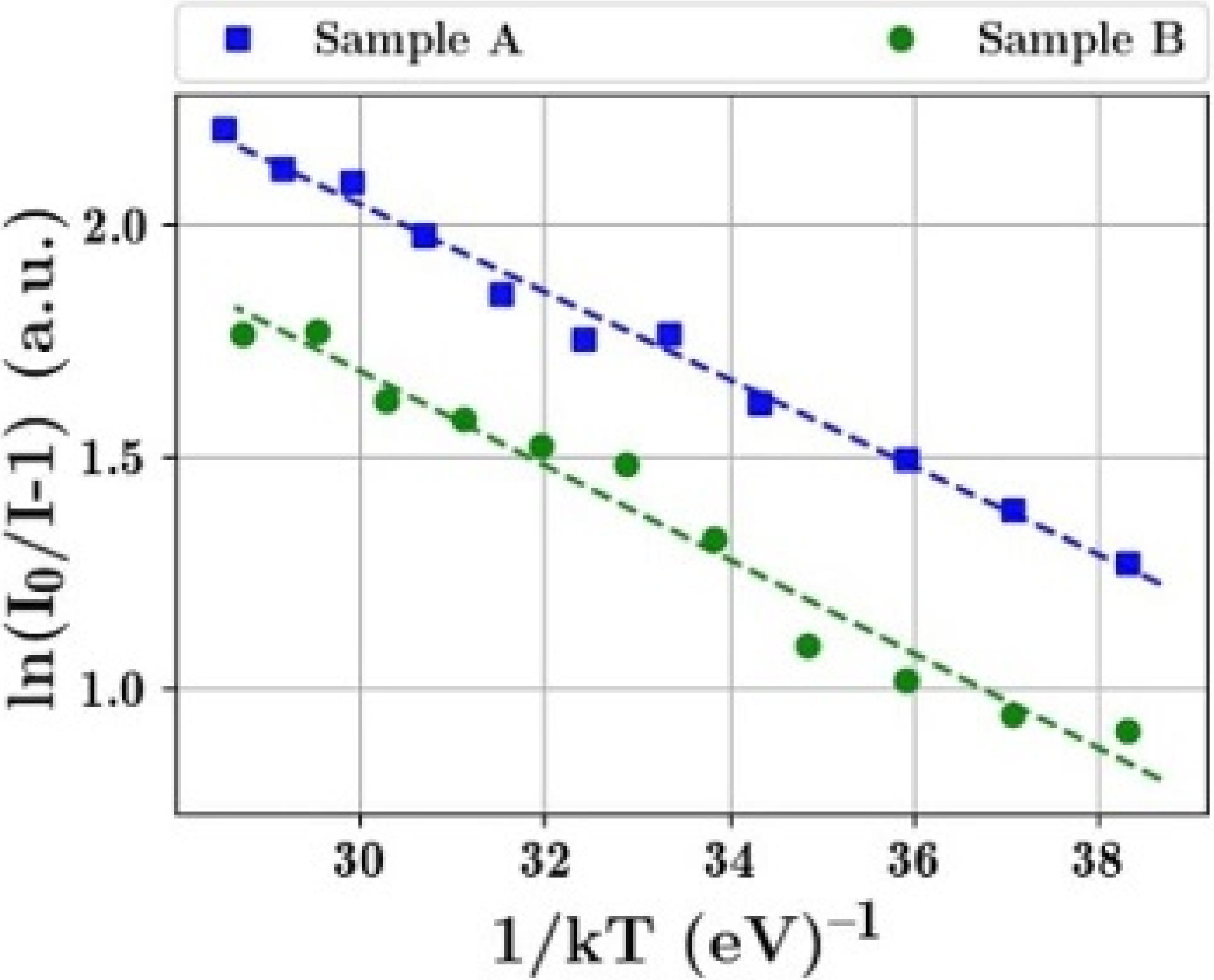
Sample A
Sample B
ln(I0/I-1) (a.u.)
2.0
1.5
1.0
30
32
34
36
38
1/kT (eV)$^{-1}$